ChemComm

COMMUNICATION

View Article Online
View Journal | View Issue

Cite this: *Chem. Commun.*, 2019, **55**, 11587

Received 26th June 2019,
Accepted 28th August 2019

DOI: 10.1039/c9cc04930d

rsc.li/chemcomm

Order–disorder transition in the $S = \frac{1}{2}$ kagome antiferromagnets claringbullite and barlowite†

Alyssa Henderson, [a] Lianyang Dong, [bc] Sananda Biswas, [d] Hannah I. Revell,[c] Yan Xin, [c] Roser Valenti, [d] John A. Schlueter*[e] and Theo Siegrist *[bc]

The transition in the quantum magnets barlowite, $Cu_4(OH)_6FBr$, and claringbullite, $Cu_4(OH)_6FCl$ is of an order–disorder type, where at ambient temperature interlayer Cu^{2+} ions are dynamically disordered over three equivalent positions. The disorder becomes static as the temperature is decreased, resulting in a lowering of symmetry. *Ab initio* density functional theory calculations explain this structural phase transition and provide insights regarding the differences between these two materials.

Quantum magnets, materials showing strong correlations and an $S = \frac{1}{2}$ spin, exploit quantum mechanical functionality that is often counterintuitive and without equivalence in the classic world. In systems where competing interactions lead to frustration, quantum fluctuations remain strong even to the lowest temperatures. The ground state of such systems, in particular two-dimensional frustrated magnets, is considered the quantum spin liquid (QSL), where no long-range order exists even at $T = 0$ K.[1,2] The proposed connection between high-temperature superconductivity and QSLs has been discussed extensively.[3–5] The expected long-range quantum entanglement and topological order in QSLs allow probing novel states of matter.[6,7]

Condensed matter phases that realize a QSL provide a synthesis challenge in solid state chemistry.[8] The search has mostly focused on $S = \frac{1}{2}$ two-dimensional spin systems in trigonal and kagome lattices, with antiferromagnetic interactions so that geometrical frustration is observed. Examples containing molecule-based $S = \frac{1}{2}$ triangular spin lattices include κ-(BEDT-TTF)$2Cu_2(CN)_3$ (BEDT-TTF = bis(ethylenedithio)tetrathiafulvalene)[9] and $EtMe_3Sb[Pd(dmit)_2]_2$ (dmit = 1,3-dithiole-2-thione-4,5-dithiolate).[10,11] Alternatively, transition metal ions can also provide $S = \frac{1}{2}$ systems, but are prone to distortions that relieve the geometrical frustration, inducing long-range magnetic order at low temperatures. Such distortions are also a concern in many kagome lattice potential QSL materials.[12]

Herbertsmithite, $ZnCu_3(OH)_6Cl_2$, is one of the few geometrically perfect kagome lattices showing strong evidence of a QSL state, where fractionalized spin excitations form a spectral continuum.[13,14] It belongs to the atacamite mineral family with composition $Zn_xCu_{4-x}(OH)_6Cl_2$. For $x = 0$, interlayer Cu^{2+} mediates magnetic interactions, resulting in long range order in the distorted kagome layers. As interlayer Cu^{2+} are replaced by Zn^{2+}, perfect kagome layers are stabilized at $x > 1/3$ (Zn-paratacamite), and magnetic order is suppressed at $x = 1$.[15,16] Single crystals have been grown successfully,[14,17] but unfortunately, potential site-disorder with Zn^{2+} substituting for Cu^{2+} in the kagome layers is reported.[18]

Claringbullite, $Cu_4(OH)_6FCl$,[19,20] and barlowite, $Cu_4(OH)_6FBr$,[21] are two related atacamite minerals with Cu^{2+} based kagome layers (Fig. S1, ESI†). While interlayer chloride coordinates to three Cu^{2+} and three hydroxyl hydrogens in herbertsmithite, replacement of half of these chloride ions with fluoride shifts the layer stacking (Fig. S2 and S3, ESI†). Thus, the electronegative fluoride resides in a hydrogen rich cavity. Strong H–F hydrogen bonding provides the likely origin of the different layer alignments.

Synthetic barlowite, recently prepared and characterized,[22–24] has a hexagonal structure at room temperature.[22] At low temperature, the interlayer Cu^{2+} ions order and induce a small distortion of the kagome layers with overall orthorhombic *Pnma* symmetry.[23] Synthetic claringbullite is isostructural to barlowite at room temperature.[25] We hypothesized that the high temperature high symmetry with perfect kagome layers is due to dynamic disorder of the interlayer Cu^{2+}. We thus investigated the temperature dependence of the crystal structures of claringbullite and barlowite to gain insight into their low-temperature structural distortions affecting the kagome layers.

[a] *Department of Physics, Florida State University, Tallahassee, FL 32310, USA*
[b] *Department of Chemical and Biomedical Engineering, FAMU-FSU College of Engineering, Tallahassee, FL 32310, USA. E-mail: siegrist@eng.famu.fsu.edu*
[c] *National High Magnetic Field Laboratory, 1800 E Paul Dirac Drive, Tallahassee, FL 32310, USA*
[d] *Institute of Theoretical Physics, Goethe University Frankfurt, 60438 Frankfurt am Main, Germany*
[e] *Division of Materials Research, National Science Foundation, Alexandria, VA 22314, USA. E-mail: JSchluet@nsf.gov*

† Electronic supplementary information (ESI) available: Supplemental figures, refinement data, and synthesis details. CCDC 1883276, 1883264 and 1882561. For ESI and crystallographic data in CIF or other electronic format see DOI: 10.1039/c9cc04930d

The room temperature crystal structures of both synthetic compounds have disordered interlayer Cu^{2+} sites, space group $P6_3/mmc$, and unit cell parameters a = 6.6699(2) Å and c = 9.1761(3) Å and a = 6.6786(2) Å and c = 9.2744(3) Å, respectively.[22,24] A study of barlowite indicated that the interlayer copper site is ordered at 100 K, resulting in an orthorhombic unit cell with symmetry $Cmcm$[23] (Fig. S4–S6, ESI†). Another study reported an even lower symmetry, *Pnma*, occurs below T = 250 K.[26] Thus, we hypothesized claringbullite may behave in a similar way.

Claringbullite: Room temperature powder X-ray diffraction data, collected at APS beamline 11-BM, was analyzed for structural models in space group $P6_3/mmc$ and $Cmcm$ (a = 6.6699 Å, $b = \sqrt{3}a$ = 11.5526 Å, and c = 9.1761 Å) but Rietveld refinements are consistent with $P6_3/mmc$ (Fig. S7, ESI†).

Single crystals of claringbullite do not show superstructure reflections between 295 K and 120 K using our laboratory diffractometer. We therefore measured three single crystals of claringbullite at 100 K and 10 K at the APS 15-BM (ChemMatCARS) beamline. In one case, no superstructure reflections were observed at 10 K, with the symmetry remaining hexagonal $P6_3/mmc$. Two samples of claringbullite showed superstructure intensities at 100 K, consistent with a single- and a multiple-domain primitive orthorhombic unit cell.

Examination of the diffraction frames from the single domain crystal showed weak superstructure reflections consistent with space group *Pnma* and unit cell parameters of a = 11.5133(2) Å, b = 9.1527(2) Å, and c = 6.6726(1) Å, with the hexagonal c-axis now the b-axis as shown in Fig. 1. The interlayer Cu^{2+} are now ordered, occupying one of the three sites above/below the triangle formed by the copper atoms in the kagome layers, which pucker by about 0.12 Å. Results of the refinement are given in Tables S2–S4 (ESI†).

The dynamic JT distortion in claringbullite develops local correlations which electron microscopy may be able to show. Claringbullite was therefore investigated by scanning transmission electron microscopy (STEM) at room temperature. High angle annular dark field (HAADF) STEM imaging along and perpendicular to the hexagonal c-axis was carried out at room temperature. Atoms in the HAADF images appear as bright dots with their intensity proportional to the square of atomic number (Z^2) and sample thickness. Fig. 2a and b show the structure projection parallel to the c-axis, revealing the stacked kagome lattices in claringbullite, where the brighter atomic columns are the Cu^{2+} in the kagome lattice. The weak intensity atoms (indicated by arrows in Fig. 2b) are the disordered interlayer Cu^{2+}, which are randomly distributed over the three possible sites. This is most apparent by looking at the structure perpendicular to c-axis, *i.e.* along the a-axis (Fig. 2c–e), where the projected positions extend over 0.182 nm (Fig. 2d), much more than for kagome layer Cu. See ESI† for more details.

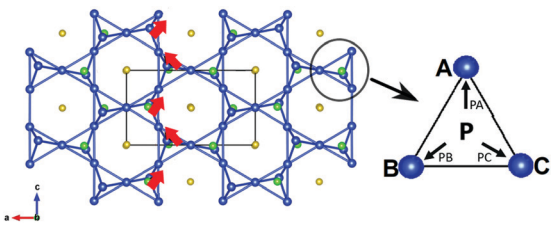

Fig. 1 Claringbullite crystal structure at 100 K in space group *Pnma*. The red arrows indicate the correlated displacement of the interlayer Cu^{2+}. Cu–Cu bonds are indicated. Color scheme: blue = Cu, yellow = F, green = Cl. Hydrogen and oxygen atoms have been omitted for clarity. (right) High symmetry position P for PES calculations.

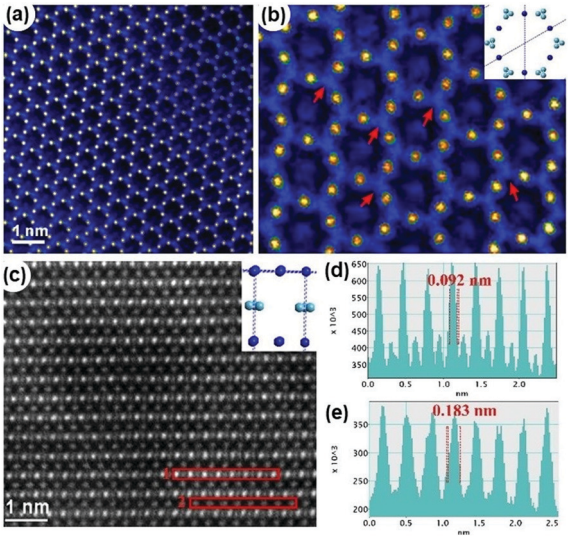

Fig. 2 (a) Atomic resolution HAADF-STEM image of claringbullite looking down [0001] c-axis; (b) enlarged and FFT-filtered [0001] image with interlayer Cu indicated by arrows; inset: corresponding projected structure schematic with kagome Cu as dark blue and interlayer Cu as light blue. (c) FFT-filtered atomic resolution images of a-axis HAADF-STEM image; inset: corresponding schematic. (d) Intensity line profile of line 1 (d) and 2 (e) of kagome Cu layer.

Barlowite: High resolution room temperature powder X-ray diffraction data (Fig. S8, ESI†) was collected at the APS 11-BM beamline and agrees with the previously reported room temperature barlowite single crystal[22] and powder[24] X-ray data showing hexagonal symmetry. The symmetry-breaking transition must occur between room temperature and 250 K.[26] The expected superstructure intensities are small compared to the substructure intensities and thus difficult to observe even in synchrotron powder diffraction. Therefore, single crystal techniques are required.

The appearance of superstructure reflections with half integer indices as a function of temperature indicates development of a primitive orthorhombic structure. The appearance of the superstructure reflection (−2, 0.5, 0) is a suitable marker for the hexagonal to primitive orthorhombic distortion. A single crystal (−2, k, 0) index scan from k = 0.4 to 1.1 includes both the superstructure reflection and the substructure reflection (−2, 1, 0), the latter serving as an intensity reference. Fig. 3 shows the temperature dependence of intensity of the (−2, 0.5, 0) reflection normalized to the (−2, 1, 0) reflection, indicating a "soft" onset of the Cu^{2+} ordering at 276 K. Short-range order is present up to about 285 K, where the superstructure intensity becomes of the order of the background (Fig. S9, ESI†). The substructure reflection (−2, 1, 0) shows broadening due to the

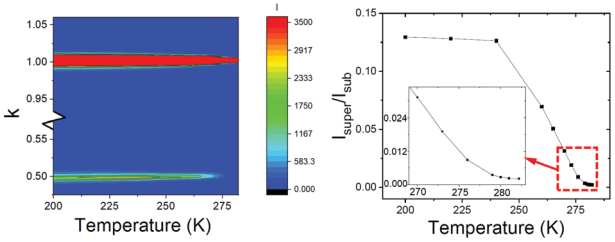

Fig. 3 (left) A (−2, *k*, 0) index scan from *k* = 0.4 to 1.1 for a single crystal of barlowite as a function of temperature. (right) Temperature dependence of the integrated intensity of the superstructure reflection (−2, 0.5, 0) for a single crystal of barlowite, normalized to the (−2, 1, 0) intensity.

inequivalence of the *a*- and *b*-lattice parameters, growing more distinct as the temperature is lowered below 273 K.

The orthorhombic distortion has implications with respect to both crystal and electronic structure. The holosymmetric coordination of the interlayer Cu^{2+} ion[21] distorts to one of three positions at low temperature. While the Jahn–Teller (JT) distortion has been extensively studied in octahedral Cu^{2+} complexes with 4 + 2 or 2 + 4 coordination, the JT effect can also occur in trigonal prismatic coordination.[27]

We thus suggest that barlowite exhibits a dynamic JT distortion at room temperature with a order–disorder transition into a low temperature *Pnma* structure at 276 K. Defects that serve as nucleation centres likely influence the observed order–disorder transition, inducing multiple twinning for the orthorhombic phase. The transition temperature is therefore sample dependent and influenced by growth conditions.

To further investigate the difference between claringbullite and barlowite and understand the origin of the different ordering temperatures, we explored the potential energy surface (PES) for the interlayer Cu^{2+}. Static density functional theory (DFT) calculations were performed in the nonmagnetic configuration considering both the room ($P6_3/mmc$) and low temperature structure (*Pnma*) parameters. To find the symmetry of the PES, the fractional occupancy of the interlayer Cu^{2+} for the hexagonal structure was removed. A PES was obtained for both systems and symmetries by comparing the total energy due to the nuclear motion of the interlayer Cu^{2+} relative to the high symmetry position P (Fig. 1). All other atoms were kept fixed at the experimentally obtained positions, taken from data reported in this paper and from literature values.[26] Calculating energies along different paths away from P, we find that the lowest energy structures always lie along either PA, PB or PC (Fig. 1 and Fig. S10, ESI†); where A, B, and C denote the projected positions of three nearest Cu atoms situated on the kagome layer. Schematics representing the calculations are shown in Fig. 4a.

Fig. 4 reveals the three-fold symmetry, which compels both systems to undergo an order–disorder transition as observed in the experiment due to the finite probability of tunnelling of the interlayer Cu atoms between three equivalent minima. Fig. 3a shows the degeneracy along PA, PB and PC. Though the other directions remain energetically higher, they still mimic the symmetry of the PES. The interlayer Cu^{2+} tunnelling frequency was estimated by fitting a potential of the form $V(x) = -Ax^2 + Bx^4$ to the

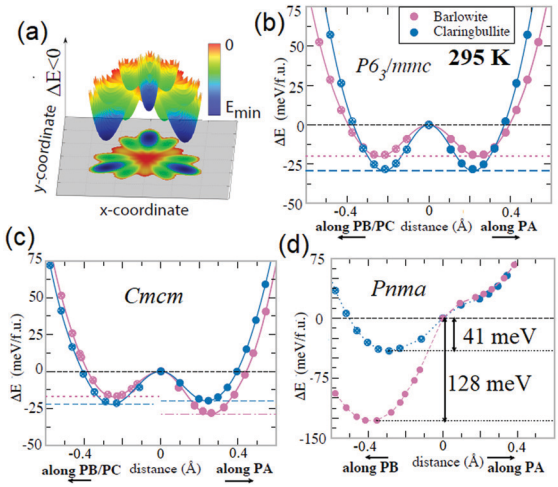

Fig. 4 Schematic of (a) 3D potential energy surface (PES) at room temperature for both systems; (b) 2D slice of the room temperature PES, and low temperature *Cmcm* (c) and *Pnma* (d) phase PES.

curve in Fig. 4b and solving an effective one-dimensional anharmonic oscillator problem. The values of tunnelling frequencies thus obtained were 9.6 meV f.u.$^{-1}$ and 13 meV f.u.$^{-1}$ for barlowite and claringbullite, respectively. These tunnelling frequencies can be measured *via* Raman spectroscopy.

Our experimental results show that the order–disorder transition occurs at a lower temperature in claringbullite than in barlowite. The calculated low temperature PESs support this view (Fig. 4c and d). We have considered both the *Cmcm* and *Pnma* symmetry for the low temperature structures for both the systems and found that *Pnma* is indeed lower in energy than *Cmcm*. While group–subgroup relationship would indicate $P6_3/mmc \rightarrow Cmcm \rightarrow Pnma$ path for the successive phase transitions as the temperature is lowered, our results indicate that the *Cmcm* might only have a very small region of stability which may be accessed dynamically over a narrow temperature range around the ordering temperature. This is in line with the experimental observation that *Pnma* "wins" over *Cmcm* even at 276 K in barlowite. The reduction in symmetry from *Cmcm* to *Pnma* is due to a slightly different ordering scheme of the interlayer Cu^{2+}.[23] The low temperature PESs show one distinct difference compared to the room temperature PES: it is asymmetric as the degeneracy gets lifted along PA and PB/PC. As all calculations are performed at $T = 0$ K, our results suggest that both systems will distort towards the *Pnma* structure at low temperatures. However, we find that the static distortion in barlowite is more stable than in claringbullite (by an energy (128–41 meV)) consistent with our experimental observation of persistence of this phase in barlowite in a wider region of temperatures than in claringbullite. This may be due to the two competing interactions: the overall metric imposed by the kagome layers themselves, and the interlayer atoms that need to find an equilibrium position. The larger Br atom mostly expands the *c*-axis, but is constrained by the kagome lattice to expand perpendicular to it. In barlowite, this anisotropic strain drives the transition to a higher temperature than claringbullite.

Finally, we investigated the electronic structure of barlowite to find the origin of the order–disorder transition in these systems. The results suggest that these materials undergo a 'Jahn–Teller like distortion' due to the instability caused by the electronic degeneracy between two sets of d-orbitals of the interlayer Cu^{2+} ion at the position P with point group symmetry C_{3v} (Fig. S11, ESI†). Thus, the system becomes unstable with respect to the nuclear motion away from P in such a way that this degeneracy is lifted.

Since the order–disorder transition may be considered as a transition from a dynamic to a static JT distortion, the details of the coordination of the interlayer Cu^{2+} are as follows: the Cu–O coordination polyhedron is trigonal prismatic, with the Cu^{2+} offset towards one side, resulting in four short bonds with distances of 1.988 Å, and two longer Cu–O bonds at 2.434 Å. Distances to the three Cu^{2+} each in the kagome layers above and below are 2.737 Å (2×), and 3.161 Å (4×). This type of distortion was described previously for the case of trigonal prismatic Cu^{2+}, with the elongated bonds in the *cis*-positions.[27] In the case of barlowite, similar Cu–O distances and distortions are observed. The static distortion is favoured in barlowite, while the dynamic distortion prevails to lower temperatures in claringbullite.

In conclusion, we have demonstrated that the room temperature structures of the kagome systems barlowite and claringbullite show dynamic disorder of the interlayer Cu^{2+}, rendering the kagome lattice of spin $\frac{1}{2}$ Cu^{2+} ions perfectly hexagonal. A transition from dynamic disorder to static order occurs at 276 K for barlowite, where the symmetry is lowered from hexagonal $P6_3/mmc$ to orthorhombic *Pnma* and the unit cell acquires a small distortion in the hexagonal (*ab*)-plane, slightly distorting the kagome lattice. This is in contrast to claringbullite, where this transition to the lower symmetry *Pnma* is at a temperature below 110 K, or even below 10 K, for selected samples. The calculated energy gain for the transition from dynamic disorder to static order are 128 meV $f.u.^{-1}$ for barlowite, and 41 meV $f.u.^{-1}$ for claringbullite. This larger energy gain and the larger PES asymmetry in barlowite indicate that ordering is favoured at higher temperatures than in claringbullite. This anisotropic strain is induced by the larger Br atom and leads to a larger overall energy gain for the observed distortion in barlowite. Therefore, the order–disorder transition occurs at a higher temperature compared to claringbullite. Defects present in a crystal may serve as nucleation centres for the order–disorder transition, resulting in a spread of transition temperatures depending on sample preparation and potentially, on cooling rates and the sample's history. While the systems are structurally almost identical, the substitution of Cl for Br affects the behaviour of the interlayer Cu^{2+} ion in an unexpected way.

We thank Dr S. Winter for helpful discussions. APS Sector 15 (ChemMatCARS) is principally supported by the NSF Divisions of Chemistry (CHE) and Materials Research (DMR) under grant NSF/CHE-1346572. Use of the APS, a DOE Office of Science User Facility at ANL, was supported under Contract No. DE-AC02-06CH11357. J. A. S. acknowledges support from the Independent Research/Development program while serving at the NSF. Work carried out at the NHMFL was supported by the NSF under grant DMR-1644779 and the State of Florida. A. H., L. D. and T. S. acknowledge funding from the NSF under grant DMR-1534818. H. I. R. thanks the NHMFL for the summer internship. R. V. acknowledges financial support from DFG Sonderforschungsbereich TRR 49.

Conflicts of interest

There are no conflicts to declare.

References

1 P. W. Anderson, *Mater. Res. Bull.*, 1973, **8**, 153.
2 L. Balents, *Nature*, 2010, **464**, 199.
3 P. A. Lee, *Science*, 2008, **321**, 1306.
4 P. A. Lee, *Rep. Prog. Phys.*, 2008, **71**, 012501.
5 B. J. Powell and R. H. McKenzie, *Rep. Prog. Phys.*, 2011, **74**, 056501.
6 P. W. Anderson, *Science*, 1987, **235**, 1196.
7 L. B. Ioffe, M. V. Feigel'man, A. Isoselevich, D. Ivanov, M. Troyer and G. Blatter, *Nature*, 2002, **415**, 503.
8 A. P. Ramirez, *Nat. Phys.*, 2008, **4**, 442.
9 Y. Shimizu, K. Miyagawa, K. Kanoda, M. Maesato and G. Saito, *Phys. Rev. Lett.*, 2003, **91**, 107001.
10 T. Itou, A. Oyamada, S. Maegawa, M. Tamura and R. Kato, *Phys. Rev. B: Condens. Matter Mater. Phys.*, 2008, **77**, 104413.
11 K. Kanoda and R. Kato, *Annu. Rev. Condens. Matter Phys.*, 2011, **2**, 167.
12 D. S. Inosov, *Adv. Phys.*, 2018, **67**, 149.
13 M. P. Shores, E. A. Nytko, B. M. Bartlett and D. G. Nocera, *J. Am. Chem. Soc.*, 2005, **127**, 13462.
14 T. H. Han, J. S. Helton, S. Chu, A. Prodi, D. K. Shingh, C. Mazzoli, P. Muller, D. G. Nocera and Y. S. Lee, *Phys. Rev. B: Condens. Matter Mater. Phys.*, 2011, **83**, 100402.
15 P. Mendels and F. Bert, *J. Phys. Soc. Jpn.*, 2010, **79**, 011001.
16 M. A. de Vries, K. V. Kamenev, W. A. Kockelmann, J. Sanchez-Benitez and A. Harrison, *Phys. Rev. Lett.*, 2008, **100**, 157205.
17 T.-H. Han, J. S. Helton, S. Chu, D. G. Nocera, J. A. Rodriguez, C. Broholm and Y. S. Lee, *Nature*, 2012, **492**, 406.
18 D. E. Freedman, T. H. Han, A. Prodi, P. Muller, Q.-z. Huang, Y.-s. Chen, S. M. Webb, Y. S. Lee, T. M. McQueen and D. G. Nocera, *J. Am. Chem. Soc.*, 2010, **132**, 16185.
19 E. E. Fejer, A. M. Clark, A. G. Couper and C. J. Elliott, *Mineral. Mag.*, 1977, **41**, 433.
20 P. C. Burns, M. A. Cooper and F. C. Hawthorne, *Can. Mineral.*, 1995, **33**, 633.
21 P. A. Williams, F. Hatert, M. Pasero and S. J. Mills, *Mineral. Mag.*, 2010, **74**, 797.
22 T.-H. Han, J. Singleton and J. A. Schlueter, *Phys. Rev. Lett.*, 2014, **113**, 227203.
23 C. M. Pasco, B. A. Trump, T. T. Tran, Z. A. Kelly, C. Hoffmann, I. Heinmaa, R. Stern and T. M. McQueen, *Phys. Rev. Mater.*, 2018, **2**, 044406.
24 R. W. Smaha, W. He, J. P. Sheckelton, J. Wen and Y. S. Lee, *J. Solid State Chem.*, 2018, **268**, 123.
25 X. Y. Yue, Z. W. Ouyang, J. F. Wang, Z. X. Wang, Z. C. Xia and Z. Z. He, *Phys. Rev. B: Condens. Matter Mater. Phys.*, 2018, **97**, 054417.
26 K. Tustain, G. J. Nilsen, C. Ritter, I. da Silva and L. Clark, *Phys. Rev. Mater.*, 2018, **2**, 111405.
27 J. Echeverría, E. Cremades, A. J. Amoroso and S. Alvarez, *Chem. Commun.*, 2009, 4242.

